

Fluid-structure modelling of a flexible lifting surface in a fluid flow

R. M. Howell¹, A. D. Lucey¹, M. W. Pitman¹

¹ *Fluid Dynamics Research Group, Curtin University of Technology, GPO Box 1987, Perth, WA 6845*
Email: A.Lucey@curtin.edu.au

Abstract: A versatile computational model is described for the two-dimensional fluid-structure interaction between a fluid flow and a thin flexible plate held at its leading edge. This fundamental system may be considered representative of many engineered or natural systems in which a plate or membrane experiences spontaneous, and often sustained, vibration. The energy exchanges between the fluid and structure that underpin such motions may be either desirable (for example in sound-production or as a fluid-energy extraction device) or damaging (for example, producing material fatigue or instability in paper-rolling processes).

The system studied requires that the governing fluid equations are solved concurrently with those of the flexible plate with compatibility of motion and continuity of stresses at the fluid-structure interface. The former is written as a kinematic boundary condition on the solution of the Laplace equation for the fluid flow. While this implies an inviscid and irrotational flow, viscous effects are implicitly included through a streamwise distribution of bound-vorticity (*i.e.* boundary-layers are assumed to be infinitely thin) and the imposition of a Kutta condition that effectively sets the correct sum of bound vorticity. Thus, the model developed is appropriate to flows with high Reynolds number that are most commonly found in applications. Continuity of stress for an inviscid fluid requires that the pressure matches the stresses due to the flexible-plate's inertial forces and its bending stiffness. Finally, as the plate moves, its changing shape means that the lift it generates - the sum of the pressure forces that drive the plate motion - also changes. This lift variation then requires that vorticity is continuously shed from the trailing edge in order to satisfy Kelvin's circulation theorem and this yields a near-field wake that influences the flow over the flexible plate.

In our computational model we deploy a boundary-element method, using first-order vortex panels, along the surface of the flexible plate. A Kutta condition is enforced at the trailing edge of the deforming surface while the Kelvin circulation theorem is used to determine the strengths of discrete Gaussian vortex blobs that are shed and then convected with the mean flow to form the downstream wake. We assume small-amplitude disturbances of the flexible plate that permits linearisation of the kinematic condition and the wake dynamics. The flexible plate is modelled by the beam equation that is solved using finite-differences. The system can then be written as a single matrix equation for the beam deflection and its time derivatives at the collocation points and a sum of wake-vortex effects. When the latter are excluded and a steady flow is assumed, system eigenmodes can be extracted using state-space methods to determine the vibration frequencies of the fluid-structure system and the stability of such oscillations. Alternatively, numerical simulations of the full system are conducted to study the response to an applied initial excitation. In this paper, we explore the effect on the stability of the fluid-loaded plate when a point mass is added to an otherwise homogeneous plate. It is shown that this effect can be either stabilising or destabilising depending upon the location of the added mass and that its inclusion modifies the energy exchanges of the fluid-structure interaction of the 'standard' system.

Keywords: *Fluid-structure interaction, flexible surface, flutter instability, modal analysis, computational modelling.*

1. INTRODUCTION

The lifting surface in the present study is a thin flexible plate that in its unloaded state is exactly aligned with the direction of a uniform flow. When subjected to a small-amplitude perturbation, the contour of the deformed plate causes it to become a lifting surface over which a non-uniform fluid pressure field acts. This serves to further deform the plate which, in turn, modifies the lift force and its associated pressure field. Thus, a fluid-structure interaction is established that may lead to either attenuating, neutrally-stable or amplifying oscillations of the structure. Of particular importance is the critical value of the flow speed at which fluid-loaded vibration first become unstable. The two-dimensional system studied is illustrated in Fig. 1(a). While this system is of fundamental interest, its dynamics underlies the behaviour of many physical systems ranging from fluttering flags, through to oscillations of the human soft-palate that create snoring noises, and to energy-harvesting devices that could extract fluid energy through its transfer to the plate in a process of controlled destabilisation.

Kornecki *et al.* (1976) were the first to conduct comprehensive modelling and analysis of the problem at hand, although it has classical roots that date back to Lord Rayleigh (and see, for example, the elegant experiments of Zhang *et al.* (2000) who investigated the oscillation of a filament in a soap-film flow). Using ideal flow Kornecki *et al.* studied the two-dimensional problem of flexible plate embedded in an infinite domain of fluid, as did the more recent work of Huang (1995), Yamaguchi *et al.* (2000), Watanabe *et al.* (2002), Argentina and Mahadevan (2005) and Tang and Païdoussis (2007).

Eloy *et al.* (2007, 2008) incorporated the effects of finite aspect ratio and showed that these principally served as a correction to the fundamentally two-dimensional dynamics of the problem. The flow-plate configuration has been extended to that of a flexible plate mounted in plane channel flow; see Aurégan and Depollier (1995) and Guo and Païdoussis (2000). All of these studies predict that the plate loses its stability through flutter that sets in beyond a critical uniform flow speed or Reynolds number in the case of viscous channel flow; for the latter refinements see Balint and Lucey (2005) and Tetlow and Lucey (2009). For short plates the flutter mode is predicted to comprise a combination of the first and second *in-vacuo* modes while for long plates, or plates with heavy fluid loading, the critical mode is dominated by higher-order mode content. The recent work of Howell *et al.* (2009) elucidated the instability mechanisms showing that ‘short’ plates succumb to single-mode flutter while ‘long’ plates are destabilised by modal-coalescence flutter of the Kelvin-Helmholtz type predicted exactly for fluid-loaded plates of infinite extent and discussed, for example, by Crighton and Oswell (1991) and Lucey *et al.* (1998).

In this paper we extend the work of Howell *et al.* (2009) to include inertial inhomogeneity in the structure and study its effect upon the stability of the flexible plate. In particular we model and investigate the effect of adding a point mass, for a range of values, at different locations along the flexible plate. Certain counter-intuitive results are obtained - for example, the addition of mass can be stabilising - and these are explained in terms of the energy transfers between the fluid and the plate. Finally, we emphasise that, although the investigation described herein has a specific focus, the methods developed and deployed have a very general application for modelling the fluid-structure interaction of an arbitrarily deforming flexible surface.

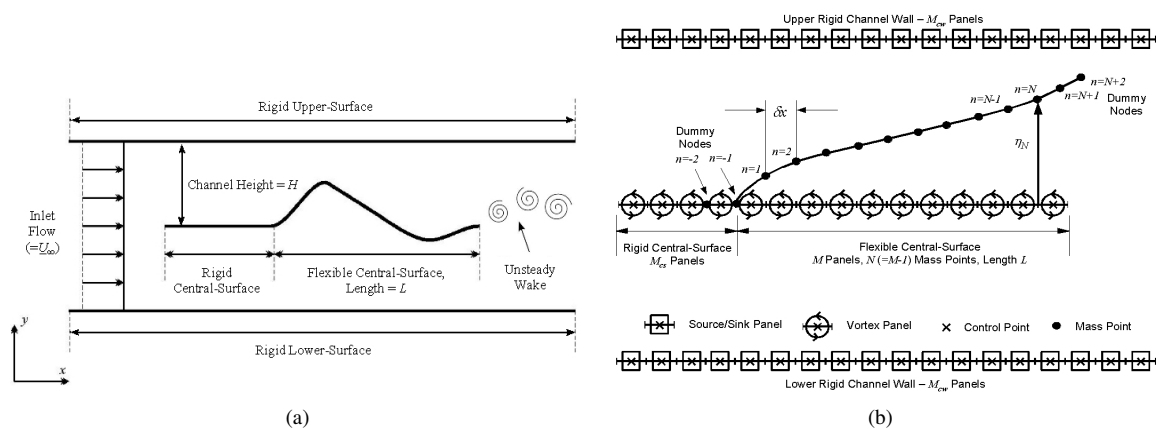


Figure 1: Schematics of (a) the system studied, and (b) the computational modelling approach used.

2. COMPUTATIONAL MODELLING

The irrotational part of the flow field is found using a linearised boundary-element method (BEM) while the vorticity shed from the trailing edge of the flexible plate is modelled using the discrete-vortex method (DVM). In the application of the BEM, first-order vortex panels are used on the rigid central surface and the flexible plate because the discontinuity of tangential fluid velocity across these thus makes them lifting surfaces. It is the distributed lift that drives the motion of the flexible plate. Source-sink panels are applied on the rigid channel walls. A schematic of the scheme is shown in Fig. 1(b). The singularity strengths are determined by enforcing the no-flux boundary condition at every panel control point and, for the central surfaces, continuity of the distributed vorticity between adjacent panels. Thus the vector of singularity strengths is given by

$$\{\Gamma_m\} = [I_{im}^N]^{-1} \{U_\infty \theta_m + \dot{\eta}_m + u_m^{Nb}\}, \quad (1)$$

where $\Gamma_m = \gamma_m + \lambda_m$ for the vortex elements. $[I_{im}^N]^{-1}$ contains, in addition to the normal influence-coefficients of the singularities, the boundary conditions of: a) vortex strength continuity at panel end points; and b) zero vorticity at the plate's trailing edge (thus enforcing the standard Kutta condition of zero pressure difference at the trailing edge for linear displacements). θ_m is the panel's angle to the horizontal, which in the linear framework is the streamwise spatial derivative of the boundary, η_m (the vertical deflection of the plate), while u_m^{Nb} is the normal component of the velocity induced by the wake vortices evaluated at control point m .

The unsteady Bernoulli equation is used to determine the pressure distribution on the flexible plate. The transmural pressure is then used as the forcing term in the one-dimensional thin flexible-plate equation couched in finite-difference form. The motion of the plate and the fluid flow are fully coupled through deflection, vertical velocity and acceleration of the two media at their interface. For the vortical wake, Gaussian vortex blobs are shed at each time-step of the plate's motion and the circulation assigned to each blob is such that the Kelvin condition is enforced. Linearised convection is adopted in the present study whereby the blob centres remain in the horizontal plane of the undisturbed plate and thus travel downstream only with the speed of the mean flow. This approach allows a single system (matrix) equation to be written as follows

$$\begin{aligned} \rho h [\mathbf{I}] \{\ddot{\eta}_m\} + d [\mathbf{I}] \{\dot{\eta}_m\} + B [\mathbf{D}_4] \{\eta_m\} &= 2\rho_f U_\infty^2 (1/\delta x) [\mathbf{B}_1^+] \{\eta_m\} \\ &+ \rho_f U_\infty (1/\delta x) [\mathbf{B}_2^+] \{\dot{\eta}_m\} + \rho_f U_\infty [\mathbf{B}_1^-] \{\dot{\eta}_m\} \\ &+ \rho_f [\mathbf{B}_2] \{\dot{\eta}_m\} \\ &- 2\rho_f U_\infty [\mathbf{B}_1] \{u_m^{Nb}\} - \rho_f [\mathbf{B}_2] \{\dot{u}_m^{Nb}\}, \end{aligned} \quad (2)$$

where $[\mathbf{B}]$ are matrices of singularity influence coefficients, $[\mathbf{D}_4]$ is a fourth-order spatial-differentiation matrix and $[\mathbf{I}]$ is the identity matrix. ρ , h , d and B are respectively, the material density, thickness, dashpot-type damping coefficient and flexural rigidity of the plate, the dynamics of which appear on the left-hand side of the equation. Uniform discretisation of the plate length L into M collocation points defines $\delta x = L/M$. The pressure perturbation that drives the plate motion appears on the right-hand side, where ρ_f and U_∞ are the fluid density and flow speed. The pressure terms in the line order of Eqn. (2) can be interpreted in the following way: Line 1 contains the deflection-based hydrodynamics stiffness; Line 2 contains the plate-induced hydrodynamic damping; Line 3 contains the plate-induced hydrodynamic inertia; and Line 4 comprises the respective contributions to hydrodynamic damping and inertia from the wake vorticity.

The formulation of Eqn. (2) is for a homogeneous flexible plate. More details of its derivation are given in Howell *et al.* (2009) who also investigated the inhomogeneous case of spatially varying flexural rigidity, B . In the present study, we investigate inertial inhomogeneity by introducing a point mass at a specific plate location x_p (where $0 < x_p < L$); its value is given in quanta, n^+ , of total plate mass (per unit width), $M^T = \rho h L$. To effect this, the element (m, m) of the identity matrix, $[\mathbf{I}]$ in Eqn. (2) becomes $(1 + n^+(M^T/\delta x))$ where $m = \text{int}[(x_p/L)M]$ is the collocation point closest to the location at which the point mass is added.

We take two approaches to the solution of Eqn. (2). First, by neglecting the wake-vortex contributions it becomes a second-order ordinary differential equation in $\{\eta\}$. Setting $w_1(t) = \eta(t)$ and $w_2(t) = \dot{\eta}(t)$ and rearranging the matrices in companion-matrix form, yields a system equation in the form

$$\dot{w} = [H]w, \text{ where } w = \{w_1, w_2\}^T. \quad (3)$$

Single-frequency time-dependent response is assumed at ω which is a complex eigenvalue of $[H]$. Positive ω_I and ω_R respectively represent the oscillatory and amplifying parts of the response.

Alternatively, we perform a time-discretisation of η in Eqn. (2) and then numerically time-step, using a semi-implicit method, the equation to determine the system response to some form of initial perturbation. In doing so we are able to study transient behaviour and reveal localised flow-structure dynamics that when summed contribute to the system response.

3. RESULTS

We non-dimensionalise using the scheme in Crighton and Oswell (1991) and Lucey *et al.* (1998) and thus

$$\bar{t} = t [\rho_f^2 B^{\frac{1}{2}} / (\rho h)^{\frac{5}{2}}], \quad \bar{U} = U_\infty [(\rho h)^{\frac{3}{2}} / (\rho_f B^{\frac{1}{2}})] \quad \text{and} \quad \bar{d} = d [(\rho h)^{\frac{3}{2}} / (\rho_f^2 B^{\frac{1}{2}})]. \quad (4a, b, c)$$

Using the time scale that appears in Eqn. (4a), angular frequencies are therefore non-dimensionalised as $\bar{\omega} = \omega [(\rho h)^{\frac{5}{2}} / \rho_f^2 B^{\frac{1}{2}}]$. The non-dimensional streamwise coordinate, the length (or mass ratio) of the flexible plate and the channel height are defined by

$$\bar{x} = x/L, \quad \bar{L} = L[\rho_f / (\rho h)] \quad \text{and} \quad \bar{H} = H[1/L]. \quad (5a, b, c)$$

Howell *et al.* (2009) showed that for $\bar{H} = 1$ the system behaves as if the flexible plate were in an infinite domain of fluid flow; *i.e.* the channel walls seen in Fig. 1 are effectively absent. This is the configuration studied herein. We also remove the upstream splitter plate and neglect structural damping, hence $\bar{d} = 0$; the effects of these refinements were presented in Howell *et al.* (2009). Thus, for the present system the non-dimensional control parameters in the investigation that follows are the flow speed \bar{U} , the plate length \bar{L} , the quantity of added mass n^+ , and its location \bar{x}_p .

To understand the results of our numerical simulations, we consider the energy evolution of the system. Adapting the derivation of Balint and Lucey (2005), the plate energy changes with time according to

$$\frac{d}{dt} \left(\underbrace{\frac{1}{2} \rho h \int_0^L \dot{\eta}^2 dx}_{E_k} + \underbrace{\frac{1}{2} n^+ M^T \dot{\eta}^2 |_{x=x_p}}_{E_k^+} + \underbrace{\frac{1}{2} B \int_0^L \eta_{,xx}^2 dx}_{E_s} \right) = \underbrace{\int_0^L (-\Delta p) \dot{\eta} dx}_{\dot{W}}, \quad (6)$$

where the total plate energy, E_t , is the sum of the kinetic energies of plate, E_k , and added mass, E_k^+ , plus the plate's strain energy, E_s . Equation (6) shows that the plate energy either grows or decays in time depending upon the rate of work done by the pressure loading, $(-\Delta p)$ (determined by the right-hand side of Eqn. (2)). In our results we present energy records, $\bar{W}(t)$, that represent the sum of pressure work done up to time t and therefore corresponds to the current value of plate energy E_t ; these are non-dimensionalised by the initial strain energy of the plate due to the applied deflection.

3.1 'Short' plates - low mass ratio

Figure 2(a) shows the variation of system eigenvalues with applied flow speed for a homogenous, or 'standard', short plate at $\bar{L} = 1$. Single-mode flutter of the second system mode is the critical instability at a non-dimensional flow speed $\bar{U} = \bar{U}_c = 5.452$. Figure 2(b) shows the numerical simulation of the critical mode at this flow speed. Note that the simulation commenced by releasing the plate from an applied deformation - the thick black line - in the shape of second *in-vacuo* mode. The critical mode, seen to contain strong contributions from the first and second *in-vacuo* modes, then evolves from the initial excitation. Howell *et al.* (2009) monitored the phase angle between the pressure loading and plate velocity in numerical simulations showing that both the leading-edge singularity and the trailing-edge Kutta condition contribute to non-orthogonality of the pressure and plate velocity. The product of these terms yields the localised rate of work done (per unit area of plate) which is then non-zero when integrated over one period of oscillation. The plate-energy record for the simulation of Fig. 2(b) is shown in Fig. 2(c). After transients due to mode adjustment have convected away, the total energy is constant. However, it is also seen that the energy exchanges between plate and flow are spatially dependent; thus for example, the third quarter from the leading edge of the flexible plate is locally unstable while the fourth quarter is stable. It is the sum of all these energy transfers that, in this case, yields the neutral stability of the system at this critical speed.

We now show how the addition of a point mass changes the results of the standard case characterised by Fig. 2. Figures 3 and 4 show the effect of adding a point mass of $n^+ = 3$ (three plate masses) at positions $\bar{x}_p = 0.625$

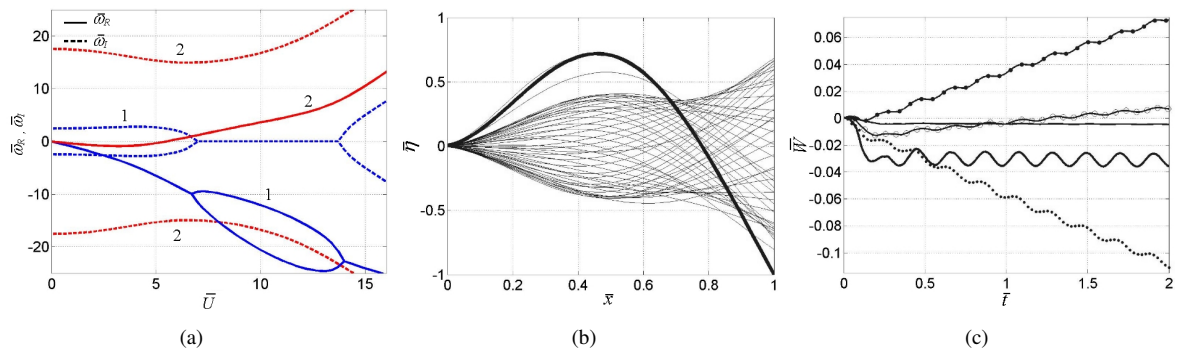


Figure 2: System dynamics for $\bar{L} = 1$:

(a) Variation of eigenvalues with flow speed (oscillatory and growth/decay parts represented by broken and full lines respectively), (b) time-sequence of instantaneous plate position at critical speed $\bar{U}_c = 5.452$ (of Mode 2 in (a)), and (c) time series of cumulative energy transferred from flow to plate in — (thin) first, \ominus second, \bullet third, and \dots fourth quarters of the plate while — (thick) is the total of these. Adapted from Howell *et al.* (2009).

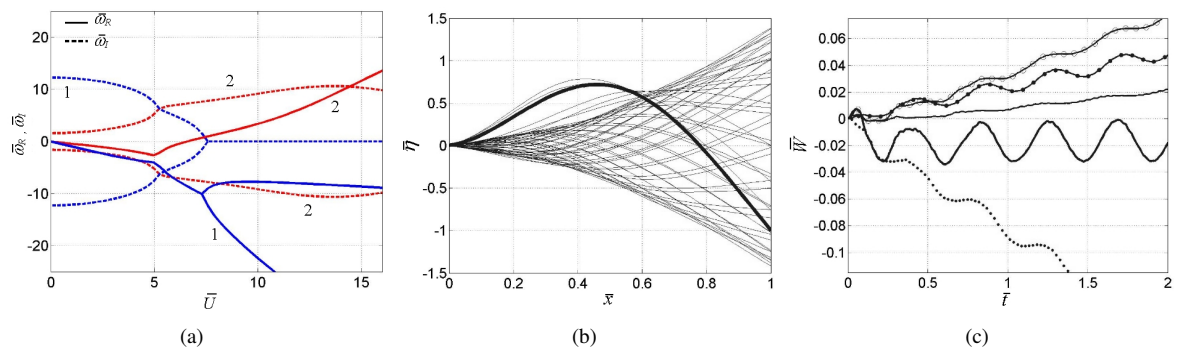


Figure 3: The effect of an added point load on the fluid-structure interaction at $\bar{L} = 1$: System giving Fig. 2 modified by added mass $n^+ = 3$ at $\bar{x}_p = 0.625$ giving $\bar{U}_c = 6.609$.

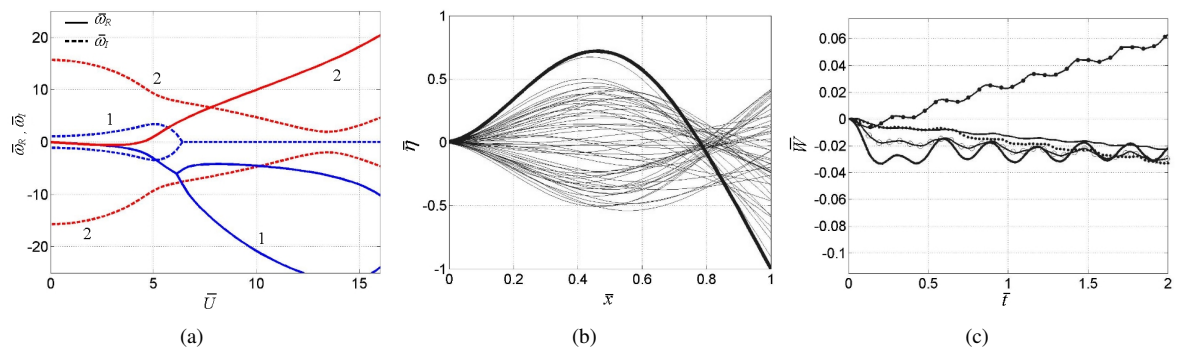


Figure 4: The effect of an added point load on the fluid-structure interaction at $\bar{L} = 1$: System giving Fig. 2 modified by added mass $n^+ = 3$ at $\bar{x}_p = 0.875$ giving $\bar{U}_c = 4.406$.

and $\bar{x}_p = 0.875$ respectively. The addition of a point mass at other locations on the plate revealed that its effect was most pronounced (for a given n^+) at these two values of \bar{x}_p . In each figure the mode and energy plots are at the critical flow speed. Adding the mass at $\bar{x}_p = 0.625$ is stabilising because it increases \bar{U}_c to 6.609. This occurs because of the reduced energy transfer to the plate in the third quarter that principally drives instability (see Fig. 2(c)). We also note from the eigenvalue plot of Fig. 3(a) that this mass addition causes coupling between Modes 1 and 2 and this interrupts the single-mode flutter mechanism of the standard case; this effect is clearly seen in the mode plot of Fig. 3(b) that strongly features a Mode-1 contribution by contrast with Fig. 2(b) in which Mode 2 is dominant.

In contrast, the same point mass added at $\bar{x}_p = 0.875$ is destabilising with the critical speed reducing to 4.406 from 5.452 of the standard case. The energy record of Fig. 4(c) shows that the added mass interrupts the stabilising effect of the fourth quarter of the plate that in the standard case of Fig. 2(c) transfers energy *from* plate *to* the fluid. However, the instability mechanism - single mode flutter - is unchanged as is evidenced by comparing the morphology of the corresponding eigenvalue plots, Figs. 2(a) and 4(a), and observing the critical modes plotted in Figs. 2(b) and 4(b).

3.2 ‘Long’ plates - high mass ratio

Howell *et al.* (2009) showed that fluid-loaded plates with high \bar{L} are destabilised by modal-coalescence flutter as opposed to single-mode flutter that gives the critical condition for plates with low \bar{L} (those investigated in §3.1 above). Figure 5 explores the effect of an added point mass to a ‘long’ plate with $\bar{L} = 10$. Without an added mass, the homogeneous case of Fig. 5(a) shows that Mode 2 is destabilised through its coupling with Mode 3. Adding a point mass with $n^+ = 0.2$ at locations $\bar{x}_p = 0.625$ and $\bar{x}_p = 0.875$ gives the eigenvalues plotted in Figs. 5(b) and 5(c) respectively. At both locations the effect is destabilising and the greatest reduction to the critical speed occurs when the added mass is placed nearest to the trailing edge of the plate. In Fig. 5(b) we note that the modal-coalescence mechanism is promoted because the added mass reduces the difference between oscillatory frequencies of the interacting modes. However, this is not the situation in Fig. 5(c) and the instability mechanism is seen to differ from that of Figs. 5(a) and 5(b). Adding the point mass at $\bar{x}_p = 0.875$ promotes single-mode flutter that is known to occur at lower flow speeds than those required to cause modal-coalescence; see the discussion of fluid-load effects in Howell *et al.* (2009). Thus, the effect of adding mass is complex because there exist two potential instability mechanisms within the fluid-structure system.

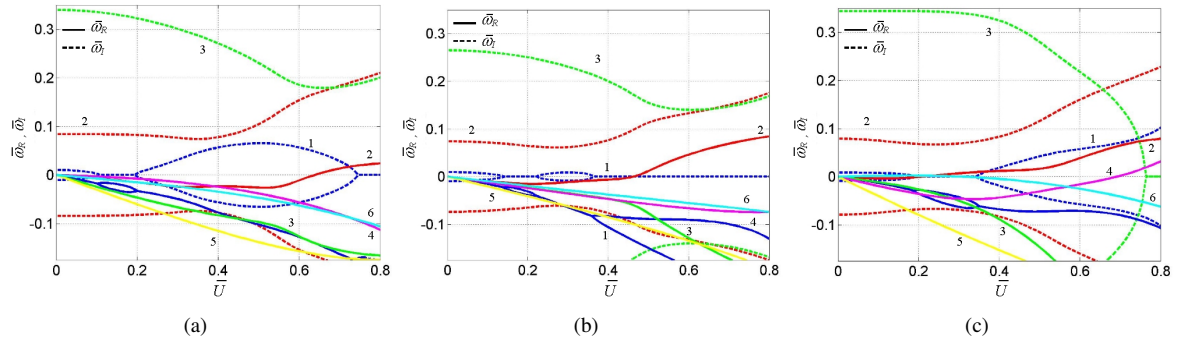


Figure 5: Variation of eigenvalues with flow speed for $\bar{L} = 10$ (oscillatory and growth/decay parts represented by broken and full lines respectively), (a) homogeneous - no added mass, and with added point mass $n^+ = 0.2$ at: (b) $\bar{x}_p = 0.625$ and (c) $\bar{x}_p = 0.875$.

3.3 Summary of critical-speed variations

The effect of the wake is not included in the investigations of §3.1 and §3.2. Thus, in Fig. 6(a) we show the variation of critical speed of a homogeneous plate (no added mass) with plate length (mass ratio), \bar{L} . For short plates the wake effect is stabilising while for long plates it is destabilising. In light of the discussions above, we can then infer that the wake inhibits single-mode flutter and promotes modal-coalescence flutter. Thus, its effect on plates with added mass would be complex given the interplay between the two types of instability noted in §3.1 and §3.2. Finally, in the absence of wake effects, we present a summary of the variation of critical

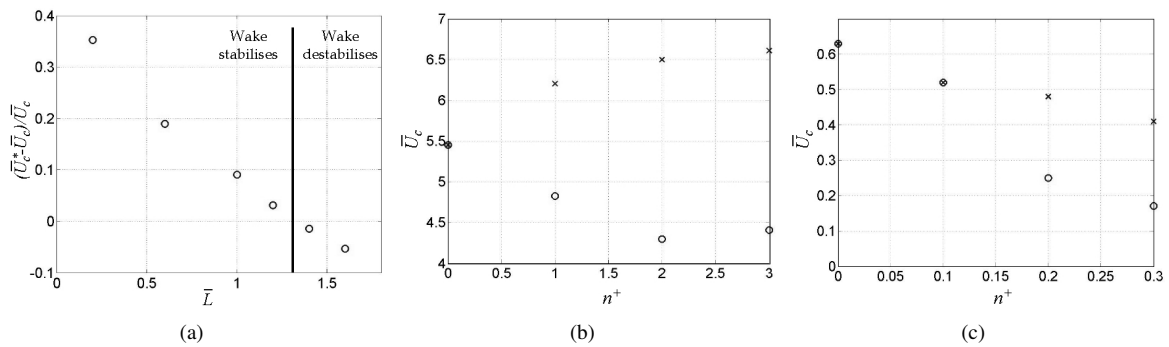


Figure 6: Effect on critical speed of: (a) wake - U_c - difference (with minus without wake) upon \bar{L} , and added point mass (no wake), for (b) $\bar{L} = 1$, and (c) $\bar{L} = 10$ added at \times , $x_p = 0.625$, and \circ , $x_p = 0.875$.

speed with added mass for ‘short’ ($\bar{L} = 1$) and ‘long’ ($\bar{L} = 10$) plates in Figs. 6(b) and 6(c) respectively. These again reinforce the finding that added mass can be either stabilising or destabilising depending upon its location and the type of instability that gives the system’s critical speed.

REFERENCES

- Argentina, M. and Mahadevan, L. (2005) Fluid-flow-induced flutter of a flag. *Proceedings of the National Academy of Sciences of the United States of America* 102(6):1829-1834.
- Aurégan, Y. and Depollier, C. (1995) Snoring: Linear stability analysis and *in vitro* experiments. *Journal of Sound and Vibration* 188(1):39-54.
- Balint, T. S. and Lucey, A. D. (2005) Instability of a cantilevered flexible plate in viscous channel flow. *Journal of Fluids and Structures* 20(7):893-912.
- Crighton, D. G. and Oswell, J. E. (1991) Fluid loading with mean flow. I. Response of an elastic plate to localized excitation. *Philosophical Transactions of the Royal Society of London A* 335:557-592.
- Eloy, C., Souilliez, C. and Schouveiler, L. (2007) Flutter of a rectangular cantilevered plate. *Journal of Fluids and Structures* 23(6):904-919.
- Eloy C., Lagrange R., Souilliez C. and Schouveiler, L. (2008) Aeroelastic instability of cantilevered flexible plates in uniform flow. *Journal of Fluid Mechanics* 611:97-106.
- Guo, C. Q. and Païdoussis, M. P. (2000) Stability of rectangular plates with free side-edges in two-dimensional inviscid channel flow. *Journal of Applied Mechanics* 67:171-176.
- Howell, R. M., Lucey, A. D., Carpenter, P. W. and Pitman, M. W. (2009) Interaction between a cantilevered-free flexible plate and ideal flow. *Journal of Fluids and Structures* doi:10.1016/j.jfluidstructs.2008.12.004.
- Huang, L. (1995) Flutter of cantilevered plates in axial flow. *Journal of Fluids and Structures* 9:127-147.
- Kornecki, A., Dowell, E. H. and O’Brien, J. (1976) On the aeroelastic instability of two-dimensional panels in uniform incompressible flow. *Journal of Sound and Vibration* 47(2):163-178.
- Lucey, A. D, Cafolla, G. J. and Carpenter, P. W. (1998) The effect of a boundary layer on the hydroelastic stability of a flexible wall. In *Proceedings of the 3rd International Conference on Engineering Hydroelasticity*, J. Horacek and I. Zolotarev, eds., Czech Technical University Press, pp. 268-273.
- Tang, L. and Païdoussis, M. P. (2007) On the instability and the post-critical behaviour of two-dimensional cantilevered flexible plates in axial flow. *Journal of Sound and Vibration* 305:97-115.
- Tetlow, G.A. and Lucey, A.D., (2009) Motions of a cantilevered flexible plate in viscous channel flow driven by a constant pressure drop. *Communications in Numerical Methods in Engineering* doi: 10.1002/cnm.1225 (invited paper).
- Watanabe, Y., Isogai, K., Suzuki, S. and Sugihara, M. (2002) A theoretical study of paper flutter. *Journal of Fluids and Structures* 16(4):543-560.
- Yamaguchi, N., Yokota, K. and Tsujimoto, Y. (2000) Flutter limits and behaviours of a flexible thin sheet in high speed flow - I: Analytical method for prediction of the sheet behaviour. *Journal of Fluids Engineering* 122:65-73.
- Zhang, J., Childress, S., Libchaber, A. and Shelley, M. (2000) Flexible filaments in a flowing soap film as a model for one-dimensional flags in a two-dimensional wind. *Nature* 408:835-839.